EVALUATION OF COLD SPRAY FOR AIRCRAFT REPAIR

Sarah E. Galyon Dorman[1], Justin W. Rausch[1] Moriah J. Ausherman[1] and Gregory A. Shoales[2]

[1]SAFE Inc, P.O. Box 3388 Monument, CO 80132, sgd@saf-engineering.com
[2]Center for Aircraft Structural Life Extension (CAStLE), 2354 Fairchild Dr, Ste 6L173, USAF Academy CO 80840

Abstract: Cold spray (CS) is being use in both civil aviation and military aircraft fleets as a method for repairing obsolete or damaged parts. There is also ongoing research funded by the United States Navy examining the ability to use CS repairs on aluminium alloys for structural applications on aircraft. Using blend out geometries relevant to aircraft damage mitigation, recent fatigue testing has shown that a CS repair of AA7050-T7451 fatigue sample geometry with a 15% to 30% blend out depths were able to improve fatigue life to near that of an undamaged fatigue sample at two stress ratios. Additional mechanical and material property testing of CS repaired coupons have shown results far exceeding those of a blend out repair, a typical aircraft repair technique. Properties such as ultimate tensile and yield strength show values similar to those of wrought. These results suggest that CS can be used for aircraft structural repair.

Keywords: Cold Spray, Structural Repair, Aluminium, Fatigue

INTRODUCTION

The U.S. Department of Defense (DoD) has listed the development of a restoration process for corroded materials in structural capacities as a current focus area [1,2]. Determining a reliable, effective and economic repair process for dimensional and structural repairs is crucial in aging aircraft sustainment. Additive manufacturing (AM) and cold spray (CS) are two manufacturing technologies that could be used to restore or manufacture obsolete aircraft structural parts.

Cold spray is a solid-state deposition repair method that deposits 5-50 μm powder particles onto a substrate. A compressed gas acts as carrier to accelerate the particles through a converging-diverging nozzle to the substrate at supersonic speeds [3]. Critical impact velocity is the velocity that is required to achieve sufficient bonding between the base material and the particle layers. CS process parameters as well as powder properties can be adjusted to achieve such velocities [4]. The type of carrier gas will also change the spray velocity. Helium is often used as a carrier gas due to its low molecular weight which allows for higher gas and particle velocity upon impact [5-7].

Historically, CS has been used as a surface coating, to aid in prevention of corrosion and surface wear. In recent years, CS has been used to make dimensional repairs to non-structural aircraft parts [8]. With the improvement shown in mechanical properties, research to prove the structural capability of CS is of high priority. R. Jones et al showed additional fatigue life when a CS patch, or doubler, was added to the coupon, increasing the cross-sectional area of the coupon [8]. Increasing the cross-sectional dimension of a part is not always an option, so testing then transitioned to a repair coupon where a divot

is machined into the coupon and then repaired with CS. Multiple researchers showed a decrease in fatigue life of repaired coupons when compared to unrepaired coupons. This is likely due to poor process parameters which lead to high porosity within the repair [9-11]. The fracture initiation location is important in determining how the load is transferred between the CS repair and the substrate as well as the mechanism of failure. B. Marzbanrad showed that tensile and compressive residual stresses led to different fatigue crack nucleation locations. As expected, typically, samples with compressive residual stresses in the substrate performed better than the sample with high tensile stress levels. The nucleation location of these samples was in the CS repair and then propagated through to the substrate. In most of the samples which had a lower fatigue life than the as received, the fracture nucleated at the CS-wrought interface [11].

Th research presented in this paper highlights the improvement in mechanical properties of CS repaired coupons when compared to un-repaired baseline coupons. Cyclic fatigue and tensile tests were completed according to ASTM standards E466 and E8 to point toward structural repair capability [12,13]. Vickers micro hardness and temperature measurements were taken to show any heat affected zones. Salt fog testing was completed according to ASTM B117 to better understand the effects of CS as a coating for corrosion protection [14].

EXPERIMENTAL METHODS

All coupons were repaired using a VRC Metal Systems (Box Elder, South Dakota, United States) Gen III cold spray system with He carrier gas. Pre-processed Solvus Global (Worchester, Massachusetts, United States) 7050 CS powder was purchased in hermetically sealed bags and used for the repair.

Fatigue Testing

Two specimen types were used for fatigue testing, a 15% blend and a 30% blend. Both coupons were manufactured from a 6.35mm (0.25 inch) thick sheet of AA7050-T7451. The 15% blend coupons are based off of the ASTM E466 fatigue coupon with a blend out in the gage that removes 15% of the coupon thickness [12]. This coupon is manufactured into pristine, having no blend out; baseline, 15% blend; repair, 15% blend repaired with CS to pristine dimensions. This coupon is beneficial in comparing the effects of damage and repairs to undamaged specimen. The sample has free edges of CS in the gage section. The 30% blend geometry has the CS repair region completely surrounded by wrought material. These two geometries allow for various CS repair geometries to be investigated. Figure 1 shows the 15% and 30% blend coupon variations.

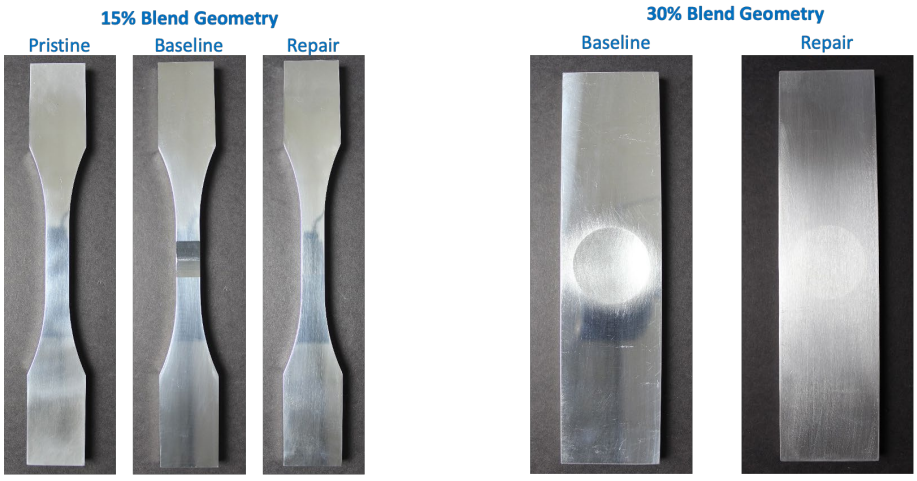

Figure 1: Fatigue testing coupons with 15% and 30% blend of the 6.35mm (0.25 inch) plate.

The 30% blend is a 50.8 mm (2 inch) by 203.2 mm (8 inch) rectangle with a 38.1 mm (1.5 inch) spherical divot in the gage. The goal of this coupon is to better represent a repair on an aircraft by having the CS repair encased by substrate on all sides. This coupon is tested as a 30% blend baseline

and CS repaired coupon. This coupon could be gaged in the area of interest to lower the risk of grip failures due to clamp up stress.

One of the variables investigated was spray raster pattern. With all other parameters the same, three different raster patterns were tested for the 30% blend repair. Figure 2 shows the three raster patterns, circular, parallel and perpendicular to the rolling direction of the wrought material. For the 15% blend most testing was completed with the parallel raster, but a small number of samples were tested with a perpendicular raster.

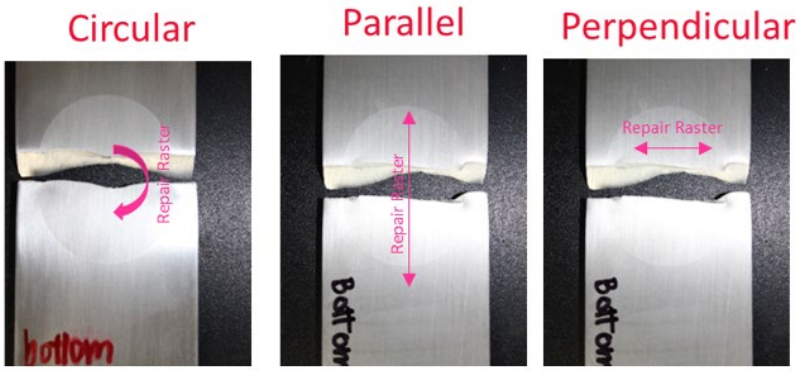

Figure 2: Spray raster direction.

A servo hydraulic test frame was used for both the 15% blend and 30% blend coupon fatigue testing. Constant load testing at a frequency of 5 Hz was completed at stresses based on percentage of the yield stress for the 15% blend samples. For the 30% blend repair, a very high stress level was used to evaluate the CS repair. Stress was calculated to compare damaged, repaired and undamaged coupons. The fatigue testing matrix is shown in Table 1 below. Gross stress is used in all cases.

Table 1: Fatigue Test Matrix.

Fatigue Test Stress (MPa)			
15% Blend		30% Spherical Blend	
R=0.1	R=-1	R=0.1	R=-1
276	177	354	237
310	221		
379	265		

Post-test the fracture surface was examined to determine fatigue initiation location, evaluate the CS for defects and follow the fatigue crack propagation through the sample. Fracture surface imaging was completed on a scanning electron microscope (SEM). Coupons were sectioned to reduce specimen length while avoiding the fracture surface. Specimens were submersed in an acetone bath within an ultrasonic cleaner. The SEM provided high magnification imaging that allowed failure nucleation location, defect size and defect location. Determination of failure initiation location and feature provides additional information about how load is transferred between the CS repair and the wrought material. Failure will nucleate at the location of highest stress concentration. Unrepaired divot coupons have the highest stress concentration at the deepest point in the divot. It is possible that CS repaired coupons could see the nucleation location move outside of the CS when the repair is carrying load equivalent to the wrought material. Likewise, if the fatigue crack is always nucleating in the bond area between the CS and base material, this could point to an issue in the bond line or suggest the cold spray is not carrying load. Fracture surface imaging was completed on all fatigue specimens.

Tensile Testing

Tensile testing was completed on untested ASTM E466 fatigue coupons as well as ASTM E8 tensile coupons [12,13]. Specimens were manufactured by machining a 15% depth divot into the wrought coupon. The specimens were then repaired with 7050 CS. Each specimen was machined to final

dimensions. All specimens were inspected by quality control before testing to ensure final dimensions, flatness, and surface finishes to mitigate stress concentrations.

An MTS 222 kN (50 kip) servo hydraulic test frame was used for all tensile testing. All testing was completed in accordance with ASTM E8 and ASTM E111 [15]. A strain rate of 0.005 mm/mm/min was used. This is the maximum allowable strain rate given in ASTM E8 for aerospace materials [13]. This strain rate was chosen due to the sensitivity of typical aerospace materials to strain hardening. CS materials are expected to behave similarly and will be tested at the same rate.

Two extensometers were placed on each face of the coupon to compare the yield stress of each side. A 35mm extensometer was placed on the wrought side of the coupon and a 50.8 mm (2 inch) extensometer was placed on the CS side. Due to the linearity of the specimen's elastic region, the extensometers were taken off after yield and the strain rate was increased for the remainder of the test.

Hardness Testing

A Vickers microhardness tester was used to compare the relative hardness of the wrought and CS. Hardness testing also showed any heat affected zones (HAZ) created during the CS process. It should be noted that because AA7050-T7451 is a precipitation hardening alloy, grain growth and other more commonly used methods for looking at a possible HAZ cannot be used. Degradation of the precipitate structure can occur at relatively low temperatures. Some work looking at friction stir welding of AA7050-T7451 was used to verify that hardness could be used to track temperature input during the CS repair process [16]. Coupons were manufactured using previously tested fatigue coupons. Sectioning was done to maximize the depth of the CS repair while avoiding the fracture surface as well as reduce the coupon to 6.35mm (0.25 in) x 12.7 mm (0.50 in) x 6.35mm (0.25 in). Specimens were then mounted and polished in accordance with standard metallographic sample preparation procedures.

Hardness measurements will be taken through the depth of the CS in multiple locations. Spacing between indents and from the edges was three indent diagonals to prevent prior indents from affecting the microhardness of subsequent indents. At completion, a 6 x 30 array of indents shall be present as shown in Figure 3.

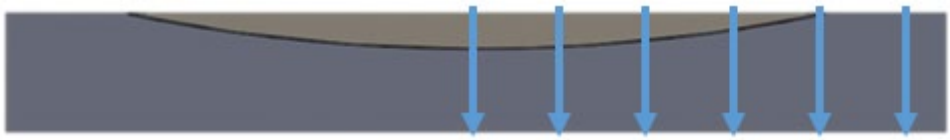

Figure 3: Microhardness testing array.

Residual Stress Measurement

Residual stress measurements were completed on the 30% repair samples for the three raster orientations. This was to address if the variation in raster direction changed the residual stresses in the samples. Both hole drilling and slitting methods were used for this measurement. The sample was slit across the area of deepest CS repair as noted by the red line in Figure 4. Only the HD1 location will be discussed as it is the location of deepest repair.

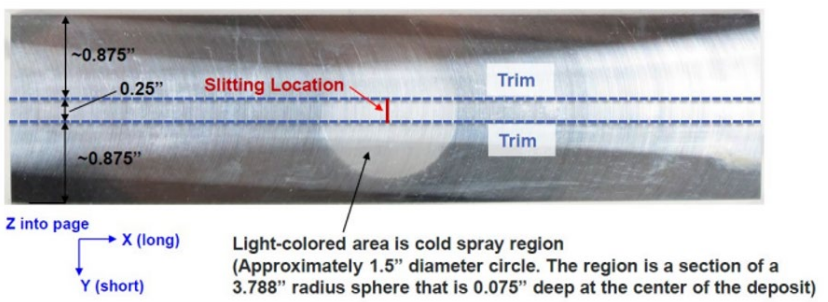

Figure 4: Residual stress meausrement location for slitting and hole drilling.

Corrosion Testing

A coupon was designed and manufactured out of AA7075 for use in testing. The coupon is 80mm x 100mm x 12.7 mm and contains four 20 mm spherical divots. The divots were repaired using two different CS processes, Process A and Process B. Both processes are optimized for mechanical performance similar to that presented in this paper. A 304SS fastener was inserted into the deepest part of the spherical CS repair. The coupon design is like that of galvanic corrosion testing coupon used for coatings evaluation [17]. High rates of corrosion are expected due to the dissimilar metals of the plate, repair, and screw. Testing was performed for 1000 hours in a salt fog chamber in accordance with ASTM B117 [14].

RESULTS

Fatigue Testing

Figure 5 shows the results of 30% blend fatigue tests performed on AA7050-T7451 for all three raster patterns compared to baseline samples and standard ASTM E466 coupons [12]. Handbook data for AA7050-T7451 is also shown [18]. Coupons were tested at a stress of 353.7 MPa (51.3 ksi) and a stress ratio (R) of 0.1. Figure 6 shows the same coupon geometry and raster patterns tested at a stress of 237.2 MPa (34.4 ksi) and a R of -1.0. The circular raster pattern performed similarly to or worse than the baseline unrepaired coupons for both stress ratios. The linear repairs showed improvement over baseline, with the perpendicular spray raster having the longest fatigue life of the repaired samples.

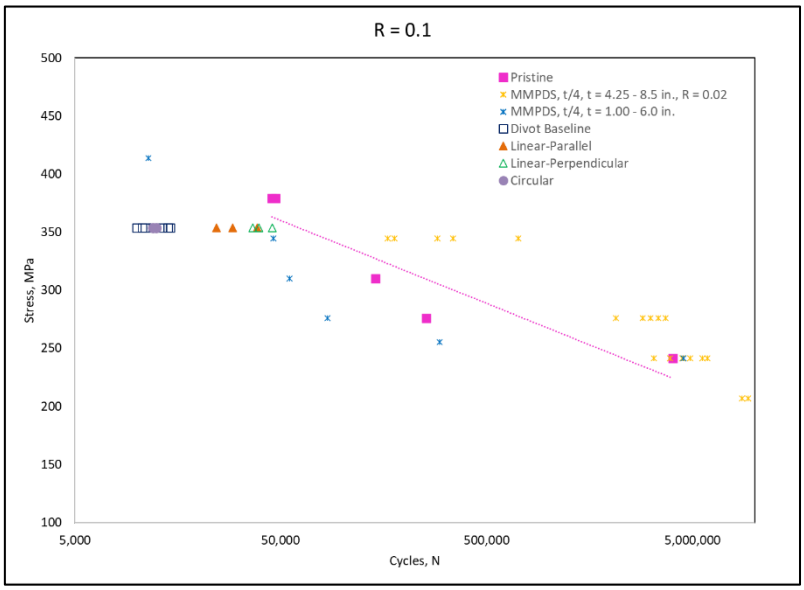

Figure 5: 30% Blend S/N Curve, R=0.1

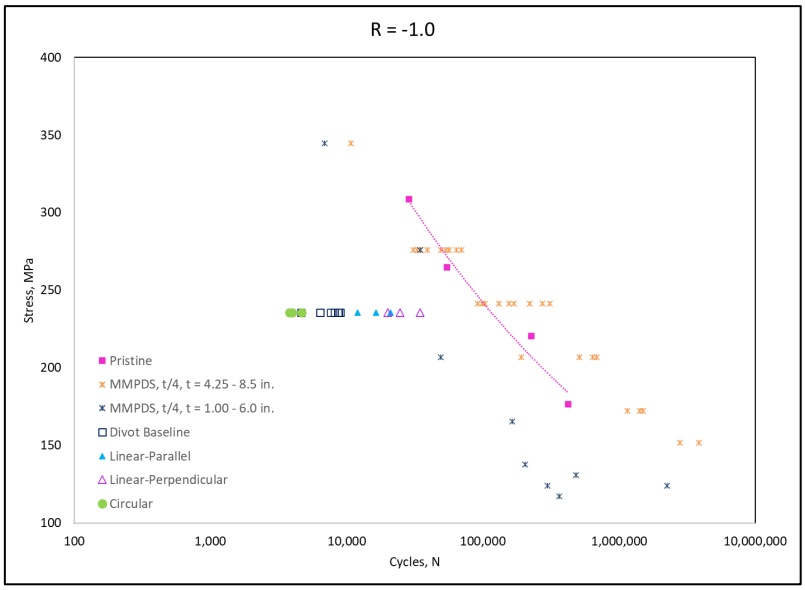

Figure 6: 30% Blend S/N Curve, R=-1

Fatigue testing was performed on 15% blend coupons. Spray validation was also performed to show that the CS repair process could be locked and repeated giving the same mechanical property results. Parallel and Validation were linear-parallel coupons sprayed months apart using the same process. Perpendicular was a linear-perpendicular raster pattern using the same machine parameters as the other sprays. A Nozzle Upgrade also occurred during the research program and was included in the validation testing on the repeatability of the CS process. The perpendicular sprays performed slightly better than the parallel as shown in Figure 7 and Figure 8. The R=0.1 shows a greater improvement with the perpendicular raster than the fully reversed loading.

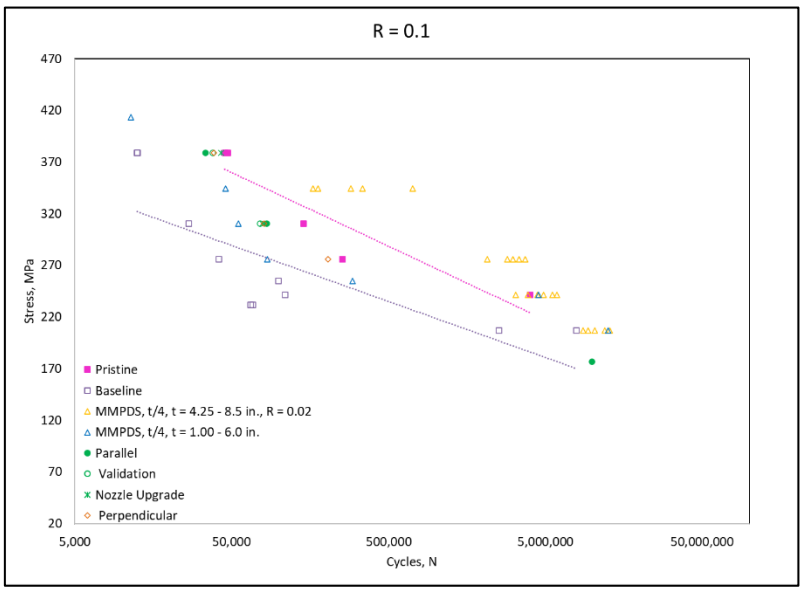

Figure 7: 15% Blend S/N Curve, R=0.1

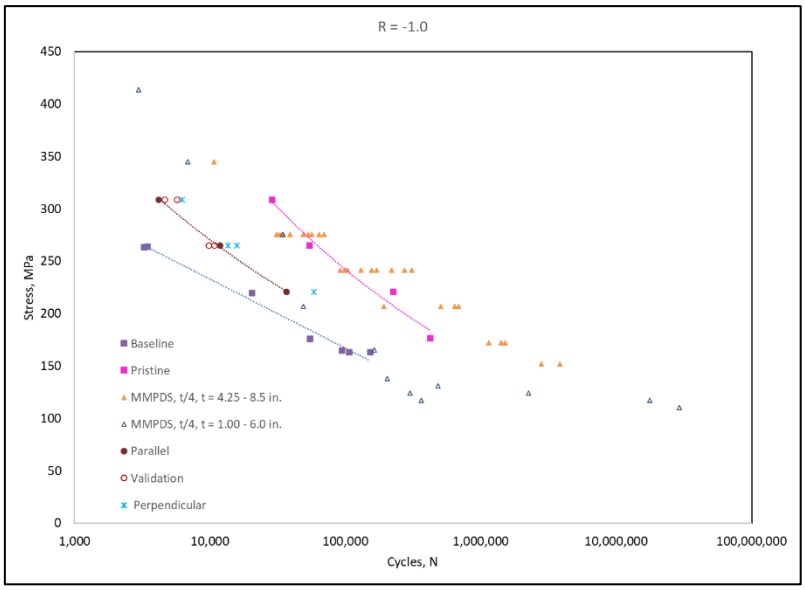

Figure 8: 15% Blend S/N Curve, R=-1

Fracture surface imaging was completed on all three CS repair raster types for the 30% divot sample. Fracture nucleation of circular coupons commonly occurred in the center of the repair. In many of the specimens, a section of incomplete bonding is present near the surface of the repair. Figure 9 shows an example of a circular repair. Sections of undeformed CS particles are present from the surface to a millimeter below the surface of the repair. An SEM image of the linear repaired coupon with the raster pattern parallel to the loading direction is shown in Figure 9. These coupons generally nucleated along the surface within the CS. The majority of the repair was well bonded with small pockets of pores in the CS. These defects caused fatigue crack initiation and then the crack propagated through the CS and into the wrought aluminium alloy prior to final failure. This correlates with the increased cycles to failure over baseline and circular repairs. The perpendicular repairs had the longest life cycle and were most likely to have grip failure. This is evidence of CS carrying load. Grip failure is an undesired effect of the improvement in mechanical properties within the CS repairs, the sample will likely be redesigned with a more standard gage section for improved fatigue resistance. Figure 9 also shows a linear repair performed perpendicular to the loading direction. This specimen nucleated in the CS just above the CS to wrought interface near the edge of the repair. The lack of pores and clear defects is further proof that the perpendicular repair showed improved properties over the other repair types.

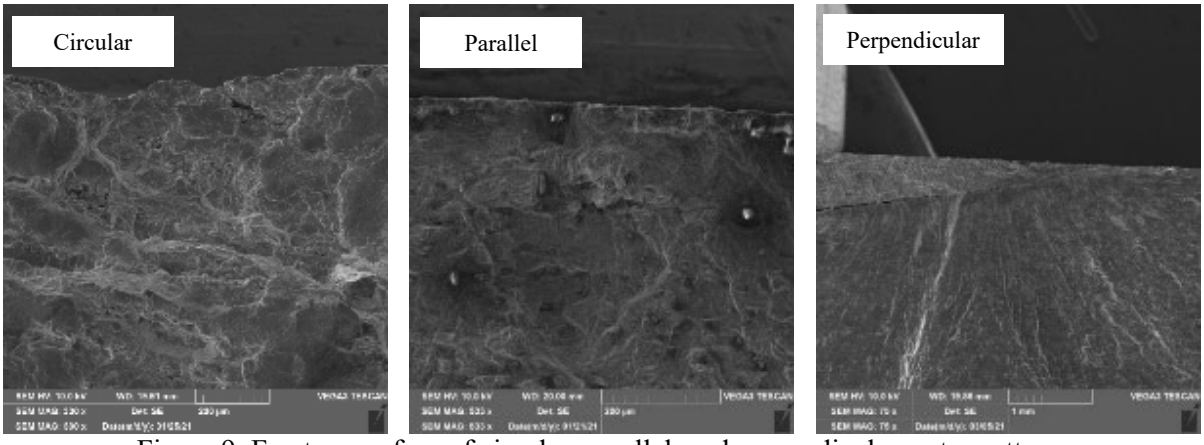

Figure 9: Fracture surface of circular, parallel, and perpendicular raster pattern.

Tensile Testing

Tensile testing of CS repaired coupons showed mechanical properties near that of wrought. Pristine coupons were tested to validate the process. AA7050-T7451 pristine E8 tensile coupons had an Ultimate Tensile Strength (UTS) of 517 MPa (75ksi), a Yield Strength (YS) of 469 MPa (68ksi), and a percent elongation of 17%. AA7050-T7451 pristine E466 fatigue coupons being use for tensile coupons had a UTS of 531 MPa (77ksi), a YS of 476 MPa (69ksi). These values correspond with the mechanical properties of industry standards [18]. The CS repaired coupons had an elongation of 5%.

The 15% CS repaired coupons had a UTS and YS that was 95% of wrought at 490 MPa (71ksi) and 448 MPa (65ksi). The stress-strain curve of both wrought and CS repaired coupons can be seen in Figure 10. Figure 11 and Figure 12 show the comparison of the yield and ultimate tensile strength of the repaired coupons to the pristine coupons.

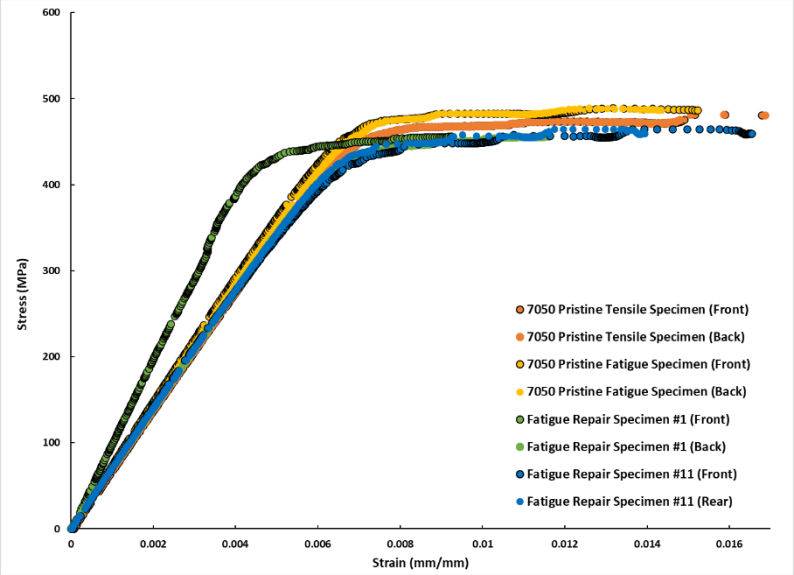

Figure 10: Stress vs. Strain of Pristine and CS repair coupons.

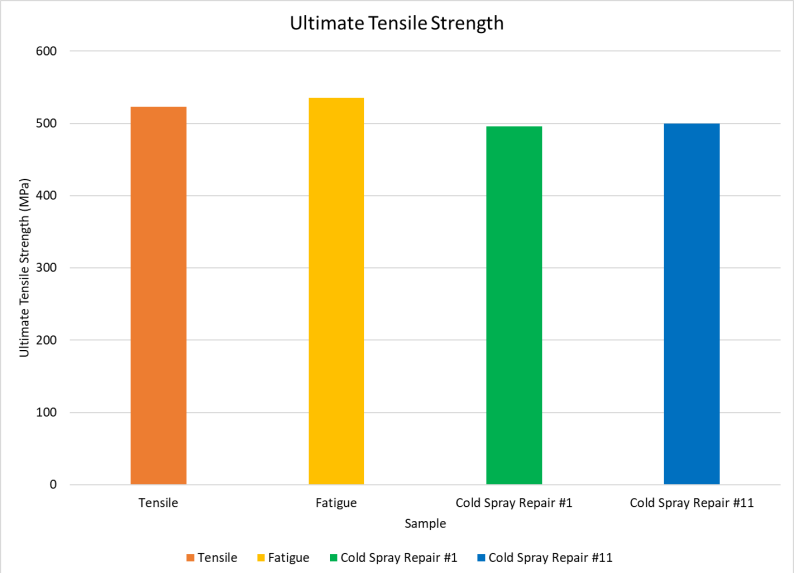

Figure 11: Ultimate Tensile Strength of pristine tensile (Tensile) and fatigue (Fatigue) coupons and 15% CS repair blend coupons (Cold Spray Repair #1 and #11)

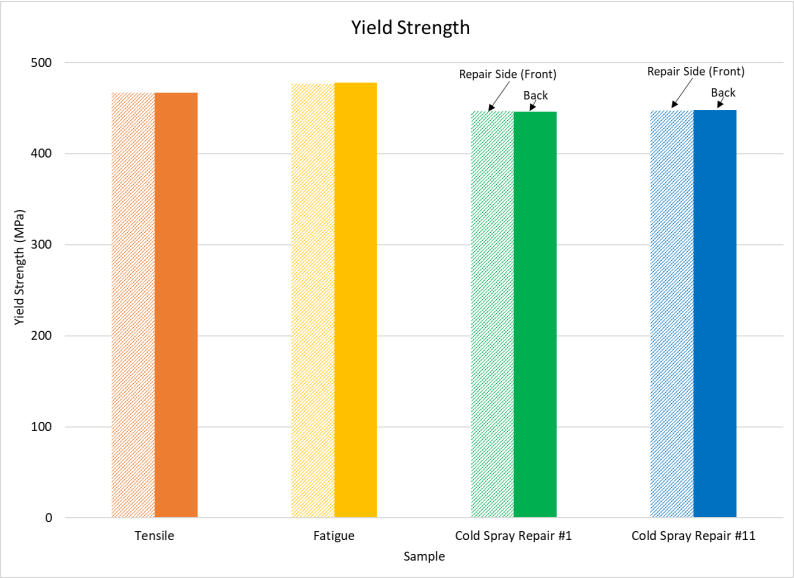

Figure 12: Yield Strength of pristine (Tensile and Fatigue) coupons and 15% CS repaired coupons

Hardness Testing

Hardness measurements were taken to compare the heat input within the CS repair as well as throughout the thickness of the specimen. Measurements were taken through the specimen thickness starting at the CS centerline. Hardness testing of wrought AA7050-T7451 gave an average of 160 HV. Although hardness testing is useful for the comparison between raster types, it should not be used to compare CS material to wrought material, as it is expected that the aluminium CS will have a lower hardness than the wrought material.

Table 2 shows the average hardness through the depth of each spray raster at different distances from the midline. The 7050 circular repairs had a Vickers hardness of 100 HV within the CS. Within the wrought material the coupons repaired by circular raster pattern decreased in hardness to 145 HV near the CS repair before returning to the expected 160 HV further from the repair. The decrease in hardness is evidence of high heat input. The Vickers microhardness of the linear repairs had increased CS hardness and a slight decrease in hardness near the wrought and CS interface, 157 HV for the parallel and 159 HV for the perpendicular raster. The increased hardness in the CS correlates well with the lack of large pores found in the linear sprays. Circular raster patterns spray in a tight circle at the bottom of the divot and work out as the divot fills. The linear sprays go from side to side, allowing for the wrought material to cool before the next layer is added limiting damage to the wrought alloy.

Table 2: Hardness average at 2mm depth

Hardness Average at 2mm Depth (just over deepest CS repair)								
Distance from Center	Midline	3mm	6mm	9mm	12mm	15mm	18mm	21mm
Linear	156	156	157	157	159	158	159	160
Circular	146	144	149	152	153	156	160	
Perpendicular	159	157	157	157	161	158	159	160

Residual Stress Measurement

The results of the slitting and hole drilling residual stress measurements, shown in Figure 13, were very similar for all three of the raster orientations. As expected, both the parallel and perpendicular raster directions have compressive residual stress at the sample surface and through the CS, then tensile residual stresses in the base aluminium alloy. The perpendicular raster has slightly more compression than the parallel raster, perhaps influencing its fatigue performance. The circular raster pattern has tensile residual stresses in the CS which may also be aiding in the crack initiation occurring in the repair center and the lack of improved fatigue life.

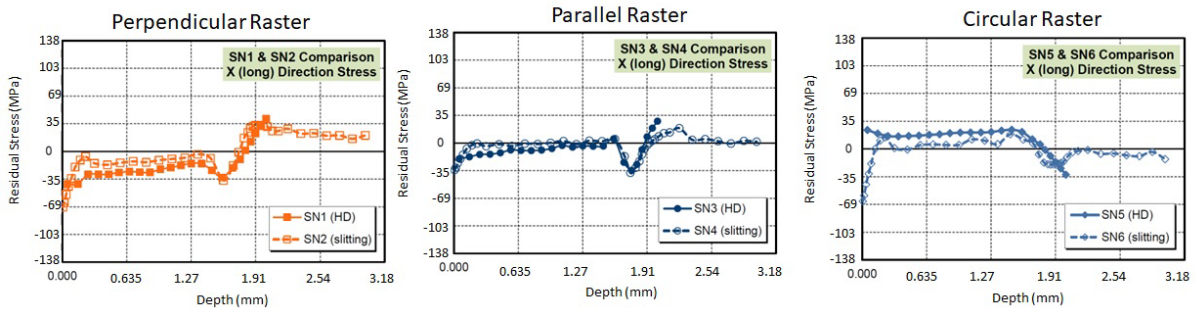

Figure 13: Comparison of residual stress measurements for each raster direction.

Corrosion Testing

Both Process A and Process B saw corrosion damage develop quickly. Figure 14 shows damage after 168 hours (1 week) of salt fog exposure. Corrosion attack is present in both the wrought aluminium and CS repair. At the four areas of CS repair, darkening and pitting are present in both processes. During testing, an area of large gelatinous corrosion product formed on the CS. This is a likely indicator of deep pits forming [19,20]. Figure 15 shows the sample after 1000 hours. The heavy corrosion product was removed from the surface by a clean water rinse. Deep pits in the CS repair area were visible after the corrosion product was removed.

Figure 14: Repaired coupon after 168 hours of exposure.

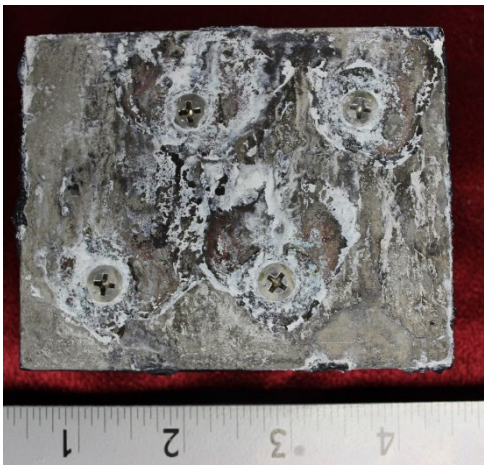

Figure 15: Repaired coupon after 1000 hours of exposure and clean water rinse.

Due to the differing grain structure of CS and wrought materials, the corrosion resistance at the interface between the two is important for structural repairs. To determine if the deep pitting damage that occurred on the surface of the coupons was present at the interface, the samples were sectioned, mounted, metallographically polished, and observed. Figure 16 show representative coupons for Process A and Process B. On both processes the wrought material showed limited damage. In the CS repaired section

pits developed, approximately 1.3mm deep. No preferential attack or undercutting was observed at the CS/wrought interface. This is consistent with prior testing on CS used for structural repairs [17,21]. Very little difference was observed between the two processes, besides Process B having multiple pits.

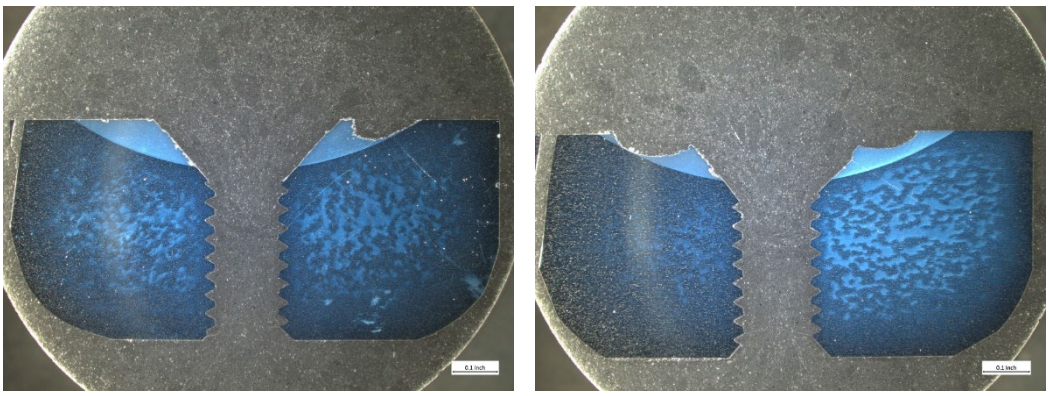

Figure 16: Process A (left) and Process B (right) cross-section after 1000 hours of salt fog exposure.

CONCLUSIONS

This research program was able to demonstrate that cold spray can be used to repair aerospace aluminium alloys. Based on these results CS can be used in certain aircraft applications as a structural repair. This program successfully showed improved CS repair properties when compared to unrepaired coupons. A common repair technique on aircraft is to blend out corrosion or defects and CS could be used to restore mechanical properties.

Repairing AA7050-T7451 divot coupons by high pressure CS resulted in increased mechanical properties when compared to unrepaired samples. The fatigue life of 15% and 30% repair coupons tested at R=0.1 and R=-1 both showed improvement. The 15% repair had ultimate and yield strength approximately 95% of the wrought material. Of the three spray raster patterns, sprays performed perpendicular to the loading direction showed the greatest improvement in fatigue life. Fatigue life improvement was greater for the 30% blend coupons where the CS was surrounded with wrought material as compared to the 15% blend that had free CS edges. In the parallel and perpendicular sprays, the majority of fatigue cracks nucleated within the CS and propagated across the interface into the wrought material.

Microhardness measurements revealed limited heat affected zones in the linear samples. This suggests the heat input is well controlled in the parallel and perpendicular spray raster. The residual stress measurements showed compressive residual stresses for the linear raster patterns in the CS, however the circular raster had tensile stress in the CS. Corrosion testing showed that CS of aluminium alloys provide cathodic protection to the repaired material. The processes tested were optimized for mechanical property performance and not corrosion resistance. Although the CS repair corroded faster than the wrought material, CS for structural repair is still considered advantageous because there is no additional galvanic attack occurring at the base material.

ACKNOWLEDGEMENTS

This work was funded under a USAFA Broad Agency Announcement FA7000-18-2-0015 by the Office of Naval Research Science and Technology. Research was completed at the United States Air Force Academy Center for Aircraft Structural Life Extension (CAStLE).

The views and conclusions contained herein are those of the authors and should not be interpreted as necessarily representing the official polices and endorsements, either expressed or implied, of the US

Air Force Academy or the US Government. This material is declared a work of the United States Government and is not subject to copyright protection in the United States.PA# USAFA-DF-2023-397 Distribution Statement A. Approved for public release: Distribution unlimited.

REFERENCES

[1] Placzankis, B.E., et al, "Evaluation of Corroison Preventative Compounds for Aviation Materials Applications," ARL TR 3457, April 2005.
[2] T.H. Van Stteenkiste, J.R. Smith, R.E. Teets, "Aluminum coatings via kinetic spray with relatively large poweder particles," *Surface and Coatings Technology,* 2002 vol. 154 (2-3), pp. 237-252.
[3] V.K. Champagne, D. Helfritch, P. Leyman, R. Lempicki, S. Grendahl, The effects of gas and metal characteristics on sprayed metal coatings. Modell. Simul. Mater. Sci. Eng., 2005, 13(7), p 1119-1128. https://doi.org/10.1088/0965-0393/13/7/008.
[4] Gilmore, R. Dykhuizen, R. Neiser, M. Smith, and T. Roemer, Particle Velocity and Deposition Efficiency in the Cold Spray Process, J. Therm. Spray Technol., 1999, 8(4), p 576–582.
[5] R.C. Dykhuizen, M.F. Smith, D.L. Gilmore, R.A. Neiser, X. Jiang, S. Sampath, Impact of High Velocity Cold Spray Particles, J. Therm. Spray Technol., 1999, 8(4), p 559-564.
[6] S.V. Klinkov, V.F. Kosarev, Measurements of Cold Spray Deposition Efficiency, J. Therm. Spray Technol., 2006, 15(3), p 364-371.
[7] K. Balani, T. Laha, A. Agarwal, J. Karthikeyan, N. Munroe, Effect of Carrier Gases on Microstructural and Electrochemical Behavior of Cold-Sprayed 1100 Aluminum Coating, Surf. Coat. Technol., 2005, 195(2), p 272-279.
[8] S. Fawaz, "Substantiation Process of Cold Spray Repaired Parts," CSAT 2017, June 14-15, 2017.
[9] B. White, "Understanding the Fatigue and Fracture Mechanisms of Cold Spray Additive Repairs," Ph.D. Thesis, University of Alabama, 2019
[10] C.M. Sample, V.K. Champagne, A.T. Nardi, D.A. Lados, Factors governing static properties and fatigue, fatigue crack growth, and fracture mechanisms in cold spray alloys and coatings/repairs: A review. Additive Manufacturing, 2020, 36, https://doi.org/10.1016/j.addma.2020.101371.
[11] B. Marzbanrad, "The effect of cold spray coating parameters on the residual stress and fatigue performance of magnesium alloys," Ph.D. Thesis, University of Waterloo, 2019
[12] "Standard Practice for Conducting Force Controlled Constant Amplitude Axial Fatigue Tests of Metallic Materials," E 466, Annual Book of ASTM Standards, 3.01, ASTM, 2015, p 1-6 .
[13] "Standard Test Methods for Tension Testing of Metallic Materials," E 8/E 8M Annual Book of ASTM Standards, 3.01, ASTM, 2022, p 1-31 .
[14] "Standard Practice for Operating Salt Spray (Fog) Apparatus," B 117, Annual Book of ASTM Standards, 3.01, ASTM 2018, p 1-11.
[15] "Standard Test Method for Young's Modulus, Tangent Modulus, and Chord Modulus," E111-17, Annual Book of ASTM Standards, 3.01, ASTM, 2017, p 1-7.
[16] R. Bush, I. Feier, and D. Diercks, "Comparison of Precipitate Structure, Modeling and Characterization in Aluminum Alloy 7050 Friction Stir Weld," Aeromet 2018, Orlando FL, May 2018
[17] J. Russell, "Galvanic Corrosion Test Method for Coatings and Materials," ASETS Defense Conference (2012), Aug 27-30, 2012, San Diego, CA.
[18] Battelle Memorial Institute, "Metallic Material Properties Development and Standardization," MMPDS-14, 2019, p 3-529.
[19] C. Bryan, "Analysis of Corrosion Residues Collected from the Aluminum Basket Rails of the High-Burnup Demonstration Cask," Sandia National Laboratory (2017) SAND2017-2306
[20] I. Huang, "Uniform Corrosion and General Dissolution of Aluminum Alloys2024-T3, 6061-T6, and 7075-T6" (2016) PhD Dissertation, The Ohio State University, Columbus, OH.
[21] A. Nardi, "VRC Metal System and Advanced Manufacturing Technologies," Cold Spray Action Team (2022), June 26, 2022, Worchester, MA